

# Structure and Mechanism of RNA Mimics of Green Fluorescent Protein

Mingxu You and Samie R. Jaffrey

Department of Pharmacology, Weill Medical College, Cornell University, New York, New York 10065; email: miy2003@med.cornell.edu, srj2003@med.cornell.edu

Annu. Rev. Biophys. 2015. 44:187–206

The *Annual Review of Biophysics* is online at [biophys.annualreviews.org](http://biophys.annualreviews.org)

This article's doi:

10.1146/annurev-biophys-060414-033954

Copyright © 2015 by Annual Reviews.

All rights reserved

## Keywords

RNA, aptamers, fluorescence, microscopy, imaging

## Abstract

RNAs have highly complex and dynamic cellular localization patterns. Technologies for imaging RNA in living cells are important for uncovering their function and regulatory pathways. One approach for imaging RNA involves genetically encoding fluorescent RNAs using RNA mimics of green fluorescent protein (GFP). These mimics are RNA aptamers that bind fluorophores resembling those naturally found in GFP and activate their fluorescence. These RNA–fluorophore complexes, including Spinach, Spinach2, and Broccoli, can be used to tag RNAs and to image their localization in living cells. In this article, we describe the generation and optimization of these aptamers, along with strategies for expanding the spectral properties of their associated RNA–fluorophore complexes. We also discuss the structural basis for the fluorescence and photophysical properties of Spinach, and we describe future prospects for designing enhanced RNA–fluorophore complexes with enhanced photostability and increased sensitivity.

## Contents

INTRODUCTION.....	188
RNA IMAGING APPROACHES.....	189
Imaging RNA with Labeled Probes.....	189
Genetically Encoded Reporters of RNA Localization.....	189
IMAGING RNA USING MIMICS OF GREEN FLUORESCENT PROTEIN....	190
Conditionally Fluorescent Small-Molecule Dyes for RNA Imaging.....	190
Identification of RNAs that Switch On the Fluorescence of Green Fluorescent Protein–Based Fluorophores.....	192
An RNA–Fluorophore Complex that Mimics Enhanced Green Fluorescent Protein?.....	193
OPTIMIZING RNA–FLUOROPHORE COMPLEXES.....	194
Directed Evolution to Generate Cell-Compatible RNA–Fluorophore Complexes..	194
Expanding the Spectral Diversity of RNA–Fluorophore Complexes Using Plug-and-Play Fluorophores.....	196
Increasing the Sensitivity of RNA Imaging.....	196
STRUCTURAL BASIS FOR SPINACH FLUORESCENCE.....	197
Structure of Spinach.....	197
Possible Mechanisms of Improved DFHBI Quantum Yield after Spinach Binding..	199
Understanding the Photobleaching Properties of Spinach.....	199
USING SPINACH AND RELATED APTAMERS FOR IMAGING	
RNA IN LIVE CELLS.....	200
FUTURE DIRECTIONS.....	201
Developing New Fluorescence Complexes Based On Non-HBI Fluorophores.....	201
Application of RNA–Fluorophore Complexes for Superresolution Imaging.....	201

## INTRODUCTION

RNA imaging is important for determining the function and regulation of noncoding and coding RNAs. Approximately 1–2% of the genome encodes mRNA, whereas the vast majority of it encodes noncoding RNAs (ncRNAs), including microRNAs, PIWI-associated RNAs (piRNAs), circular RNAs, long intergenic ncRNAs, and small nucleolar RNAs (snoRNAs) (2, 16, 26).

Most of these ncRNAs are mysterious, and their sequences often provide little information about their potential function. This contrasts with mRNAs where sequence analysis is important for predicting the encoded protein. For ncRNAs, however, the sequence usually does not provide information that predicts function. Therefore, one of the first experiments that can provide insight into the function of an ncRNA is to determine its subcellular localization. For example, nuclear ncRNAs may have a role in regulating gene transcription, whereas cytoplasmic ncRNAs likely affect processes in this compartment. The dynamics of ncRNA localization can also provide insights into its function. Translocation of an ncRNA to a specific subcellular site or structure, such as Cajal bodies in the nucleus or P-bodies in the cytoplasm, can provide insights into possible functions or regulatory pathways for the ncRNA under study.

In addition to knowledge gained from imaging ncRNAs, information on the regulation of mRNA can be gained by studying mRNA localization in cells. mRNA is subjected to a wide range of posttranscriptional processing events, including splicing, RNA editing, exonucleolytic and endonucleolytic degradation, nonsense-mediated decay, adenosine methylation, pseudouridylation,

and deadenylation (11, 42, 47). mRNAs transit through different parts of the cell as they are processed by these different pathways (1, 35, 56). Because mRNA regulatory mechanisms appear to occur in spatially defined regions or structures in cells, imaging approaches can provide insights into the pathways that regulate transcription, modification, and degradation of specific mRNAs in cells.

Altered RNA localization can also cause disease (6). For instance, fragile X syndrome, the most common genetic form of mental retardation, is associated with the loss of an RNA-trafficking protein (5). Thus, imaging approaches that reveal RNA trafficking or localization could provide insights into the underlying mechanisms of this and similar diseases.

## RNA IMAGING APPROACHES

### Imaging RNA with Labeled Probes

One can obtain real-time localization of RNA in living cells using chemical labeling approaches such as RNA synthesis with fluorescent nucleotides. These labeled RNAs are then microinjected into cells (60), and their fate is determined using fluorescence microscopy. However, this approach is limited by low throughput and by the difficulty of preparing these RNAs and microinjecting them into cells.

Molecular beacons are also used to image RNAs in living cells. Molecular beacons are oligonucleotides that typically contain both a fluorophore and a quencher (61). The beacon folds into a stem-loop structure that is nonfluorescent owing to the proximity of the fluorophore and quencher at either end of the oligonucleotide, that is, at the base of the stem. When an mRNA that has complementarity to the loop of the beacon hybridizes to the beacon, the stem is disrupted, separating the quencher and fluorophore and leading to fluorescence. Each mRNA requires a custom-designed beacon, however, and transfected beacons can exhibit nonspecific nuclear sequestration (43, 61). These issues can prevent adoption by many scientific laboratories.

### Genetically Encoded Reporters of RNA Localization

Because of the difficulties associated with the chemical labeling approaches described above, numerous groups have developed genetically encoded reporters of RNA localization (8, 30, 62). Genetic encodability bypasses the complexities of synthesis and the toxicities associated with microinjection, and genetically encoded tools can be expressed directly in cells after a DNA sequence is introduced. Genetic encoding also enables reporters to be expressed in a cell type-specific or tissue-specific manner. Thus, genetic encoding markedly simplifies imaging.

The most commonly used genetically encoded RNA imaging technique is the green fluorescent protein (GFP)–MS2 system (8). This technique uses two components: MS2, a phage protein, which is fused to GFP, and MS2 binding RNA sequences that are inserted into the 3' untranslated regions (UTRs) of mRNAs of interest. GFP–MS2 and MS2 element-containing RNAs are expressed in cells, and GFP–MS2 binds to the MS2 element-tagged RNA. Fluorescence in these cells derives from RNA–GFP complexes. Because unbound GFP–MS2 molecules diffuse throughout the cytosol, however, there can be fluorescence background that results from unbound GFP–MS2. To reduce this problem, the GFP–MS2 fusion protein is engineered to contain a nuclear localization signal (NLS) that causes excess GFP–MS2 to move into the nucleus (8). Variations of this protocol that use different RNA binding elements and fluorescent proteins have also been reported (30).

GFP–MS2 can potentially affect the localization of the mRNA to which it is bound (60) because it contains an NLS trafficking element. Indeed, because most heterologously expressed RNAs are designed to bind 24–48 GFP–MS2 sequences, each RNA is subjected to the effects of 24–48

---

**Aptamer:** short DNA or RNA sequences that fold into specific shapes that bind other molecules

**Selective enrichment of ligands by exponential enrichment**

**(SELEX):** a technique to isolate DNA or RNA that specifically binds to a target ligand

**Bioorthogonal:**

a molecule or reaction that neither affects nor is affected by cellular biochemical processes or molecules

---

NLS-targeting elements (60). In addition, because the GFP–MS2 accumulates in the nucleus, an intense nuclear fluorescence can arise and complicate the analysis of nuclear-localized RNAs. Although these issues can be addressed by careful control of GFP–MS2 expression, the system for controlling such expression can be complex to implement.

Other related approaches have been described. One involves the expression of GFP as two halves, each of which is fused to half of an RNA binding protein, eIF4A (eukaryotic initiation factor 4A) (62). RNAs that contain the eIF4A binding site nucleate the binding of the eIF4A halves, juxtaposing the two GFP halves and enabling the formation of a stable GFP complex. As the GFP complex requires ~30 min to mature into a fluorescent form (41), this method might not enable visualization of newly synthesized RNAs. Moreover, once the fluorescent complex has formed, it can spontaneously dissociate or accumulate in the cytoplasm after RNA degradation, possibly leading to high background cytoplasmic fluorescence. Thus, although this approach has high potential for use in imaging RNA in living cells, some of the potential challenges associated with it could limit its application. The approaches described above are useful for RNA imaging in live cells [as are others that were not described here owing to space limitations (60)], but they are complicated by the need to introduce different components into cells at highly specific stoichiometries.

## IMAGING RNA USING MIMICS OF GREEN FLUORESCENT PROTEIN

### Conditionally Fluorescent Small-Molecule Dyes for RNA Imaging

A simpler approach is to express an RNA tagged with a sequence that confers the fluorescence needed for imaging. This approach is analogous to GFP tagging of proteins. Short RNA sequences that fold into specific shapes that bind other molecules are termed aptamers. RNA aptamers can be generated readily using the SELEX (selective enrichment of ligands by exponential enrichment) technique, which we describe in more detail below. RNA aptamers have been developed that bind fluorescent dyes such as fluorescein (32, 52), but these aptamers have not been widely adopted for use in live-cell experiments because both the bound and unbound dyes are fluorescent.

Our strategy was to identify fluorophores that would be switched on (exhibit fluorescence) only when bound to a highly specific aptamer (46). Although many molecules exhibit fluorescence that can be induced by binding to various intracellular molecules (for example, ethidium bromide and Hoechst dyes become fluorescent upon binding nucleic acids), our strategy sought to identify fluorophores that are both switchable and bioorthogonal, meaning that the fluorescence is not switched on by normal cellular biomolecules. Selecting for this quality ensures that the unbound fluorophore is nonfluorescent and does not contribute to background fluorescence.

We sought to identify fluorophores that would not exhibit fluorescence upon interaction with normal cellular constituents but that would potentially be activated by specific RNA aptamers. We considered small-molecule dyes with structural features that could make them prone to exhibiting increased fluorescence upon rigidification, such as stilbenes (38), triphenylmethane dyes (e.g., pararosaniline and malachite green) (15), and cyanine dyes. Unfortunately, however, these dyes exhibit fluorescence activation when applied to cells, which is consistent with the known induction of fluorescence in malachite green and stilbenes by contact with lipids and membranes (23, 38). In addition, some molecules exhibit cytotoxicity at low micromolar concentrations. For example, malachite green generates cytotoxic radicals upon irradiation (7), leading to destruction of the RNA aptamers that bind it (21). Such destruction is problematic because malachite green is fluorescent when bound to cognate aptamers (3). Thus, the undesirable features of this dye have prevented the use of these otherwise potentially useful aptamers for RNA imaging.

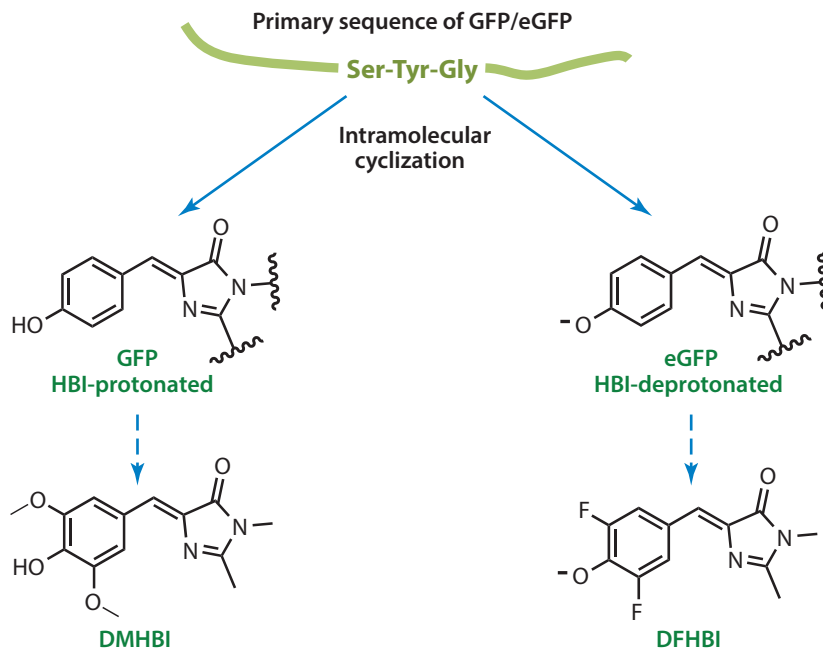


**Figure 1**

Structures of the green fluorescent protein (GFP) fluorophore and of fluorophores that are switched on by RNA aptamers. The fluorophores in GFP and in its close variant, enhanced GFP (eGFP), are derived from a Ser-Tyr-Gly tripeptide within the protein. The folded protein catalyzes an intramolecular cyclization that converts the tripeptide into the HBI fluorophore. In eGFP, unlike in GFP, the fluorophore is predominantly in the deprotonated, or phenolate, form; this form accounts for the higher extinction coefficient and brightness of eGFP. RNA mimics of GFP bind to fluorophores resembling HBI. The original RNA aptamers were designed to bind DMHBI, which resembles HBI in GFP in that the fluorophore is predominantly protonated (*left*). The DFHBI fluorophore was designed to overcome this problem and was designed as a biomimetic of the fluorophore in eGFP (*right*). Owing to the addition of fluorines, the DFHBI fluorophore is deprotonated at neutral pH. Thus, RNA aptamers that bind DFHBI, such as Spinach, Spinach2, and Broccoli, are highly bright, in part because of the higher extinction coefficient of DFHBI. Abbreviations: DFHBI, (Z)-4-(3,5-difluoro-4-hydroxybenzylidene)-1,2-dimethyl-1H-imidazol-5(4H)-one; DMHBI, (Z)-4-(3,5-dimethoxy-4-hydroxybenzylidene)-1,2-dimethyl-1H-imidazol-5(4H)-one; HBI, 4-hydroxy-benzylidene-imidazolinone.

We therefore considered the fluorophore that is formed within GFP, as this protein also exhibits conditional fluorescence. After GFP is synthesized, it undergoes an autocatalytic intramolecular cyclization reaction that involves an internal Ser-Tyr-Gly tripeptide (14). The cyclized product is subsequently oxidized to the final 4-hydroxy-benzylidene-imidazolinone (HBI) fluorophore (**Figure 1**). The oxidation results in delocalization of the  $\pi$ -electron system.

Surprisingly, when this fluorophore is chemically synthesized, it is nonfluorescent (44). Similarly, denatured GFP is nonfluorescent, and the fluorescence returns upon protein renaturation (9). The basis for the conditional fluorescence of GFP is due to the chemical structure of the fluorophore. After photoexcitation, a molecule can dissipate the energy of the excited state either through a radiative (i.e., fluorescence) pathway or through a nonradiative pathway, which usually involves vibrational or other intramolecular movements. In folded GFP, the excited-state fluorophore dissipates its energy by radiative decay (fluorescence) (**Figure 2**) (40). GFP unfolding allows the fluorophore to dissipate its energy by various bond rotations, however, and these

**Conditional fluorescence:** the emitted radiation that occurs only when some conditions or requirements are met

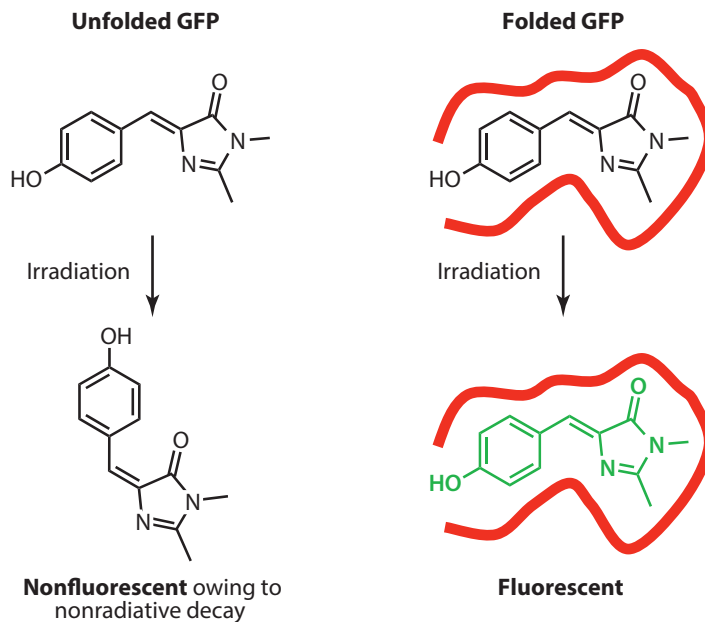


**Figure 2**

Fluorescence of green fluorescent protein (GFP) depends on the presence of protein contacts surrounding the fluorophore. GFP exhibits conditional fluorescence that depends on the folded state of the protein. When the protein is unfolded (*left*), the fluorophore portion of the protein undergoes an isomerization in response to irradiation. The folded state of the protein (*right*) inhibits this nonradiative decay pathway for dissipation of the energy of the excited state of the fluorophore. Instead, the major pathway available for the fluorophore to dissipate the energy of its excited state is fluorescence. RNA aptamers such as Spinach and Broccoli mimic the protein-suppressing effect of GFP for DFHBI [(Z)-4-(3,5-difluoro-4-hydroxybenzylidene)-1,2-dimethyl-1H-imidazol-5(4H)-one] and related GFP-like fluorophores.

rotations likely involve a twisting motion about the ethylenic bridge referred to as a “hula twist” that results in a *cis-trans* isomerization (4). The folded GFP protein prevents these motions, thereby making the radiative decay pathway the major means of dissipating the energy of the excited state fluorophore (Figure 2) (4, 40). Indeed, GFP variants that permit conformational freedom of the fluorophore have normal fluorophore maturation but reduced fluorescence (37).

One key experiment (44) tested the idea that fluorophore rigidification is essential for fluorescence using artificial restriction of bond movement by immobilizing the fluorophore in ethanol glass (ethanol at 77K). This treatment transformed the fluorophore into an intensely fluorescent species, in contrast to the fluorophore in ethanol solution at 25°C, which is nonfluorescent (44). Thus, the GFP contains a conditionally fluorescent fluorophore for which fluorescence arises because of immobilization induced by the GFP protein.

### Identification of RNAs that Switch On the Fluorescence of Green Fluorescent Protein-Based Fluorophores

We asked whether an RNA aptamer could immobilize the GFP fluorophore in a fluorescent conformation similar to what is seen in GFP. We synthesized a variety of GFP-like fluorophores, including novel ones with potentially useful spectral properties. The synthesis of the GFP fluorophore, HBI [(Z)-4-(4-hydroxybenzylidene)-1,2-dimethyl-1H-imidazol-5(4H)-one],

was described by several groups (36, 44). The main protocol for HBI synthesis is based on the work of Kojima et al. (36), and it involves an aldol condensation of *N*-acetylglycine and substituted benzaldehydes, resulting in the lactone intermediate shown in **Figure 2**. This lactone is then aminolyzed and cyclized to form the final HBI-like molecule. We made several derivatives of HBI using various substituted benzaldehydes as starting materials, and we used various acylated forms of glycine to make further derivatives. These substituents might serve as so-called handles that could help the RNA to bind the fluorophore and thereby facilitate rigidification. In addition, creation of multiple derivatives allows preparation of multiple RNA–fluorophore complexes, each of which has a different fluorescent color due to the presence of a different RNA-bound fluorophore.

HBI-like fluorophores were synthesized in two forms: (*a*) a form for use in cell-based experiments and (*b*) a form with an aminohexyl linker for immobilization on beads; this linker is required to obtain RNA aptamers in SELEX experiments. We used SELEX, a procedure that generates RNA aptamers that bind diverse types of small molecules and proteins (18), to generate RNA aptamers that bind HBI-like fluorophores. In this procedure,  $10^{14}$ – $10^{15}$  different RNAs of random sequence are synthesized and incubated with agarose beads that contain the target molecule of interest, which was a GFP-like fluorophore in this case. After extensive washing, RNAs that remain bound to the target molecule are eluted using buffer that contains the fluorophore. The eluted RNAs are then amplified by reverse transcription-polymerase chain reaction (RT-PCR) and transcribed to RNA. The binding and RT-PCR steps are repeated several times to select for the aptamers with the highest affinities. Because the RNA library has a high combinatorial diversity and RNAs have the ability to fold into diverse tertiary structures, this procedure often yields 10–100 different RNA aptamers for any given ligand (20). SELEX rarely fails to yield an aptamer that binds to a ligand target (20).

We tested whether RNA aptamers could induce fluorescence in GFP-based fluorophores. We initially focused on DMHBI [(*Z*)-4-(3,5-dimethoxy-4-hydroxybenzylidene)-1,2-dimethyl-1H-imidazol-5(4H)-one] (**Figure 1**) because this fluorophore exhibits an intense yellow-green fluorescence when immobilized in ethanol glass. DMHBI was coupled to agarose beads, and SELEX was performed to recover RNA aptamers. Of several hundred different DMHBI binding RNA aptamers tested, only a few were capable of inducing DMHBI fluorescence (46). However, these experiments did demonstrate that RNA aptamers can switch on the fluorescence of HBI-like fluorophores. To further test this concept, we generated RNA aptamers against a series of other HBI-like fluorophores and again identified aptamers capable of activating various structural derivatives of HBI (46). Taken together, these data show that RNA aptamers can switch on the fluorescence of HBI-like fluorophores and form RNA–fluorophore complexes that mimic GFP.

### **An RNA–Fluorophore Complex that Mimics Enhanced Green Fluorescent Protein?**

The excitation and emission spectra of the first RNA–fluorophore complexes resembled those of GFP, not enhanced GFP (eGFP) (46). The difference between these proteins is due to the protonation state of the HBI fluorophore. In GFP, the fluorophore is predominantly in its protonated, or phenol, form, whereas in eGFP, the fluorophore is predominantly in its deprotonated, or phenolate, form (**Figure 1**) (59). Each form has its own absorbance peak; the phenol form has an absorbance maximum at  $\sim 390$  nm, and the phenolate has an absorbance maximum at  $\sim 475$  nm. Importantly, the phenolate form of the fluorophore has a significantly higher extinction coefficient than the phenol form does, and, as the degree of fluorescence depends on the extinction coefficient and the quantum yield, eGFP exhibits higher fluorescence than GFP (59).

---

#### **Extinction coefficient:**

a measurement of how efficiently a sample absorbs light at a given wavelength

**Quantum yield:** the number of photons emitted per photon absorbed by a given fluorophore

---

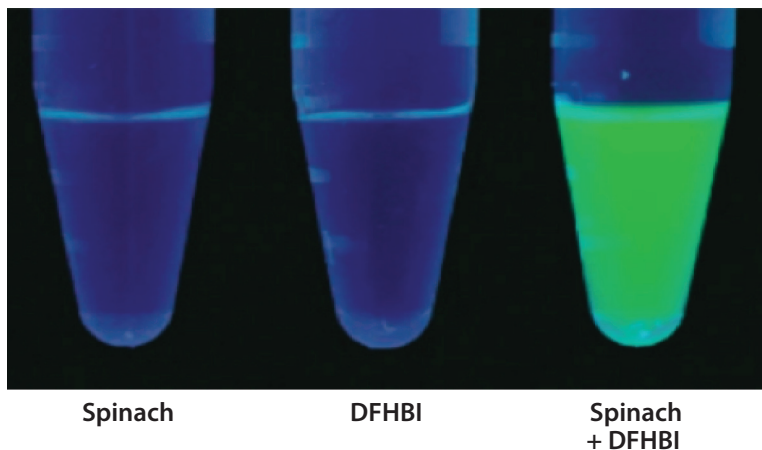


**Figure 3**

Fluorescence of the Spinach–DFHBI complex. The Spinach RNA aptamer robustly activates the fluorescence of DFHBI. Each tube contains the indicated solution, and all tubes were irradiated at 365 nm. Only the tube containing both Spinach and DFHBI exhibits fluorescence following irradiation. Abbreviation: DFHBI, (Z)-4-(3,5-difluoro-4-hydroxybenzylidene)-1,2-dimethyl-1H-imidazol-5(4H)-one.

Because the absorbance spectra of RNA–DMHBI complexes indicated that the fluorophore was in the phenol form, these RNA–fluorophore complexes were similar to the original GFP rather than to eGFP (46). We therefore used a biomimetic strategy to create an RNA mimic of eGFP. To do this, we synthesized a new fluorophore that contains a phenolate, resembling the form of the fluorophore normally found in eGFP. To ensure that the new fluorophore, DFHBI [(Z)-4-(3,5-difluoro-4-hydroxybenzylidene)-1,2-dimethyl-1H-imidazol-5(4H)-one], remained in the phenolate form, it was synthesized to contain fluorine atoms (**Figure 1**). The fluorine atoms lower the  $pK_a$  of the phenolic proton to 5.5, compared with 8.1 for HBI (46). This ensures that the fluorophore will present the phenolate state at physiological pH, including at the pH used for generating aptamers via SELEX.

We used SELEX to identify RNA aptamers that bind and switch on the fluorescence of DFHBI (**Figure 3**). The most efficient aptamer binds DFHBI with a  $K_d$  of  $\sim 500$  nM and exhibits high fluorescence: Its quantum yield is 0.72, and its total molar brightness is equal to half that of eGFP. Control RNAs, such as cellular RNA, tRNA, or scrambled RNA sequences, exhibit no fluorescence upon incubation with DFHBI. Because this RNA–fluorophore complex is very similar to GFP, we named it after the vegetable spinach, in analogy to the fruits that have been used in naming fluorescent proteins (46).

## OPTIMIZING RNA–FLUOROPHORE COMPLEXES

### Directed Evolution to Generate Cell-Compatible RNA–Fluorophore Complexes

One of the major challenges in working with RNA aptamers is that they often fail to function as expected in living cells. Once expressed in cells, aptamers are susceptible to RNA degradation and often fail to fold (39). Misfolding can result from competing folding pathways, thermal instability, or dependence on high magnesium ion concentrations that are not normally found in cells (49, 67). In addition, adjacent sequences in a target RNA into which an aptamer is inserted can interfere with folding (39, 57).

Analysis of Spinach showed that it exhibits poor folding in vitro and in cells (57). As a result, the overall fluorescence in Spinach-expressing cells was reduced. To address this, Spinach was systematically mutagenized to identify mutations that resulted in improved folding in vitro (57). Thus, an enhanced version of Spinach, designated Spinach2, exhibits improved cellular fluorescence due to improved folding (57).

Because it is difficult to identify mutations that improve folding, using selection protocols that produce aptamers that are already highly efficient at folding in cells is desirable. Thus, we modified the standard SELEX protocol to use bead-bound fluorophores for the initial rounds of aptamer selection and to use fluorescence screening to select for aptamers that exhibit fluorescence in cells (19). The fluorescence screening is performed by expressing the aptamers in *Escherichia coli*, followed by fluorescence-activated cell sorting (FACS). As these aptamers already exhibit fluorescence in cells, this selection process isolates those aptamers that show a combination of high fluorescence, high folding in cells, and compatibility with cellular ion concentrations.

After identification, aptamers can be further optimized for cellular performance by a process called directed evolution. In this approach, parent aptamer sequences are used to guide the synthesis of random libraries designed to resemble the parent aptamer. This process is similar to one previously described for ribozyme and aptamer mutant libraries (22, 29). Briefly, a DNA library is synthesized in which each encoded aptamer resembles the parent aptamer. At each position, every nucleotide has a controlled probability of being converted into one of the other three nucleotides, and this probability is mathematically calculated such that the resulting DNA library encodes all aptamers that differ from the parent aptamer by all possible 1-, 2-, 3-, 4-, 5-, 6-, 7-, or 8-nucleotide (nt) changes (19). The library is then subjected to one or two rounds of SELEX to remove aptamers that are incapable of binding the fluorophore, and the remaining aptamers are expressed in *E. coli* and processed using FACS to identify the best mutants. This procedure provides a simple method to test every possible aptamer mutant that has a similar overall sequence to that of the parent aptamer.

We used this approach to develop Broccoli, a 49-nt aptamer that exhibits bright green fluorescence upon binding DFHBI or DFHBI-1T [(Z)-4-(3,5-difluoro-4-hydroxybenzylidene)-2-methyl-1-(2,2,2-trifluoroethyl)-1H-imidazol-5(4H)-one] (19). Similar to Spinach2, Broccoli exhibits a high folding efficiency in vitro, but it shows markedly lower magnesium dependence for folding (19). In addition, Broccoli shows increased thermostability and is substantially shorter than Spinach2. The reduced magnesium dependence contributes to a nearly twofold increase in brightness in *E. coli* and allows robust imaging of tagged RNA in mammalian cells, without requiring magnesium supplementation in media (19). Broccoli may also be more resistant to cellular ribonucleases, allowing more Broccoli to be expressed in cells and ultimately leading to the increased fluorescence responsible for its selection. Thus, a combination of desirable features can be identified using selection in live cells (19).

Interestingly, unlike Spinach2, Broccoli does not require the use of a tRNA scaffold to promote its folding in vivo. This feature is highly advantageous because the tRNA scaffold can be recognized by cellular ribonucleases, possibly leading to aptamer cleavage and thereby limiting the overall fluorescence of an aptamer (49). These facts show that aptamer selection in living cells can produce aptamers that are so well folded that they do not require folding scaffolds.

Conceivably, directed evolution can lead to new photophysical properties, such as improved photostability or altered fluorescence emission spectra. For example, one could select the aptamers based on the presence of a red-shifted emission. Thus, the directed evolution approach described above could be used to identify distinct RNA aptamers that “tune” the fluorescence emission of a fluorophore.

---

**Directed evolution:**  
an approach to causing evolution of a nucleic acid or protein via selecting mutants that confer specific desirable properties

---

## Expanding the Spectral Diversity of RNA–Fluorophore Complexes Using Plug-and-Play Fluorophores

The spectral properties of Spinach and Spinach2 are determined by their fluorophore, DFHBI, which exhibits an excitation maximum at 447 nm (55). However, filters commonly used for green fluorescence in fluorescence microscopes typically illuminate cells with ~480-nm radiation. As a result, Spinach–DFHBI complexes are inefficiently excited and exhibit suboptimal brightness in typical microscopy setups. This issue was addressed by designing novel DFHBI-like fluorophores that bind Spinach but exhibit altered excitation and emission maxima (55). A structure–activity relationship analysis of DFHBI showed that altering or adding halogen substituents on the benzylidene moiety did not markedly alter the fluorescence properties of altered compounds relative to those of DFHBI, although adding substituents on the imidazolinone moiety did result in Spinach–fluorophore complexes with altered spectral properties. For example, N-1 substitutions on the imidazolinone ring, including those involving trifluoroethyl and aminoethyl substituents, resulted in red-shifted excitation and emission spectra. Specifically, DFHBI-1T bound to Spinach and exhibited a 35-nm red shift in the excitation peak and a slight red shift in the emission peak. Similar spectral properties were also observed for Broccoli–DFHBI complexes (19). As a second example, substitution at the C-2 position of the imidazolinone ring also caused marked red shifts in the fluorescence emission spectra: DFHBI-2T [(Z)-4-(3,5-difluoro-4-hydroxybenzylidene)-1-methyl-2-(trifluoromethyl)-1H-imidazol-5(4H)-one] bound to Spinach2 and exhibited a 53-nm red shift in the excitation maximum and a 22-nm red shift in the emission maximum, although the overall brightness was somewhat reduced owing to a decrease in the quantum yield (55). The increase in  $K_D$  to ~1.2  $\mu\text{M}$  suggests that the bulky trifluoromethyl moiety in DFHBI-2T may exhibit steric hindrance with the Spinach2 aptamer.

Because the spectral properties of Spinach2–DFHBI-1T more closely match those needed for commonly used filter sets, Spinach2–DFHBI-1T is efficiently excited and exhibits increased fluorescence in cells (55). In addition to improved excitation, DFHBI-1T exhibits lower background fluorescence than does DFHBI, which already exhibited low background fluorescence in cells (55).

The modified fluorophores described above not only have improved brightness during fluorescence microscopic imaging but also provide the user with an opportunity to obtain fluorescence signals that are specific for different applications. These so-called plug-and-play fluorophores can alter the spectral properties of Spinach2 by simply adding different fluorophores to the culture media, allowing the spectral properties to be adjusted based on the specific spectral needs of the experiment.

Creation of additional fluorophores may also be possible; such fluorophores might include compounds that exhibit red fluorescence. The fluorophores in various red fluorescent proteins contain substitutions at the C-2 position that extend the  $\pi$ -bond delocalization (12). Fluorophores containing similar modifications may be capable of binding to Spinach and exhibiting red fluorescence.

## Increasing the Sensitivity of RNA Imaging

An important research goal is imaging low-abundance RNAs in cells. The RNAs that have been imaged to date are expressed at high levels and form aggregates in either the cytosol or nucleus. In many cases, however, cellular RNAs are not present in aggregates, so imaging them would not benefit from a highly localized concentration of imaging tags. To increase the sensitivity, red fluorescent RNA–fluorophore complexes can be developed. Because there is less cellular autofluorescence in the red channel, imaging using a red RNA–fluorophore complex will likely have greater sensitivity than imaging using green tags. In addition, the use of fluorophores with

higher extinction coefficients and higher quantum yields will result in higher brightness and sensitivity.

Another approach to increase the sensitivity of imaging is to tag RNA molecules with cassettes containing as many as 4, 8, 16, or even more aptamer tags. An important concern with regard to this approach is to ensure that the aptamers do not hybridize with each other in the same RNA. Such hybridization could potentially occur if the strands from one aptamer interact with the complementary strand in another aptamer. Thus, judicious insertion of mutations in each aptamer could help prevent interaptamer hybridization.

## STRUCTURAL BASIS FOR SPINACH FLUORESCENCE

### Structure of Spinach

The crystal structure of Spinach bound to DFHBI provides insights into the mechanism of RNA-induced fluorescence activation of DFHBI (34, 65). The 2.8-Å resolution structure shows that Spinach folds into a single coaxial helical stack. This stack contains an irregular junction that comprises three stacked tetrads: two potassium-stabilized G-quartets stacked above a mixed-sequence tetrad (**Figure 4**) (65). These tetrads constitute the Spinach G-quadruplex, which is unique among G-quadruplexes in that (*a*) the guanine residues are distant in sequence, and (*b*) it lacks the parallel folding topology seen for other RNA G-quadruplexes.

The DFHBI fluorophore is fully planar when bound to Spinach and is sandwiched between the top G-quartet and a planar U-A-U base triple (**Figure 4**) (65). In addition to these interactions, Spinach also makes contacts with DFHBI on the plane of its rings. The imidazolone oxygen and nitrogens exhibit hydrogen bonding with the RNA. Similarly, the phenolate oxygen of DFHBI hydrogen bonds with the RNA and with RNA-bound water, and each of the fluorine atoms coordinates two water molecules. The negative charges of the phenolate are surrounded by seven RNA phosphates that lie within an approximately 8-Å radius. This high concentration of negative charge appears to attract diffuse cations and to bridge RNA functional groups, waters, and DFHBI. These coordinated cations likely account for the selectivity of Spinach for the anionic form of DFHBI (65).

The structure of Spinach bound to DFHBI is similar to the GFP fluorophore (34, 65) in that both fluorophores have a planar configuration, which maximizes fluorescence by maintaining  $\pi$ -electron conjugation across the entire fluorophore. However, Spinach and GFP differ in how they achieve fluorophore planarity: Spinach stacks planar heterocyclic bases on each face of DFHBI, whereas GFP relies on van der Waals contacts with aliphatic moieties to conformationally restrain the chromophore, thereby inducing fluorescence (51, 59). In addition, GFP utilizes buried, ionizable amino acids to interact with the fluorophore (51), whereas Spinach binds DFHBI with formally neutral moieties and cations close to the fluorophore. This binding mechanism can allow the fluorescence of Spinach to be modulated by soluble cations. Another notable difference between Spinach and GFP is that the Spinach-bound DFHBI is partially accessible to bulk solvent, unlike the deeply buried HBI fluorophore in GFP (45, 66). This solvent accessibility enables DFHBI dissociation and association, but it may also permit fluorophore quenching by oxygen or other cytosolic constituents.

G-quadruplexes may be particularly well suited to inducing the fluorescence of HBI-like fluorophores because these quadruplexes provide a highly stable, flat, hydrophobic surface that is not readily obtained by other RNA structures. For example, structures such as conventional Watson–Crick base pairs or base triples often exhibit a degree of propeller twist (13). The G-quartet can also hydrogen bond to functional groups on the edges of the fluorophore (65), and its surface is

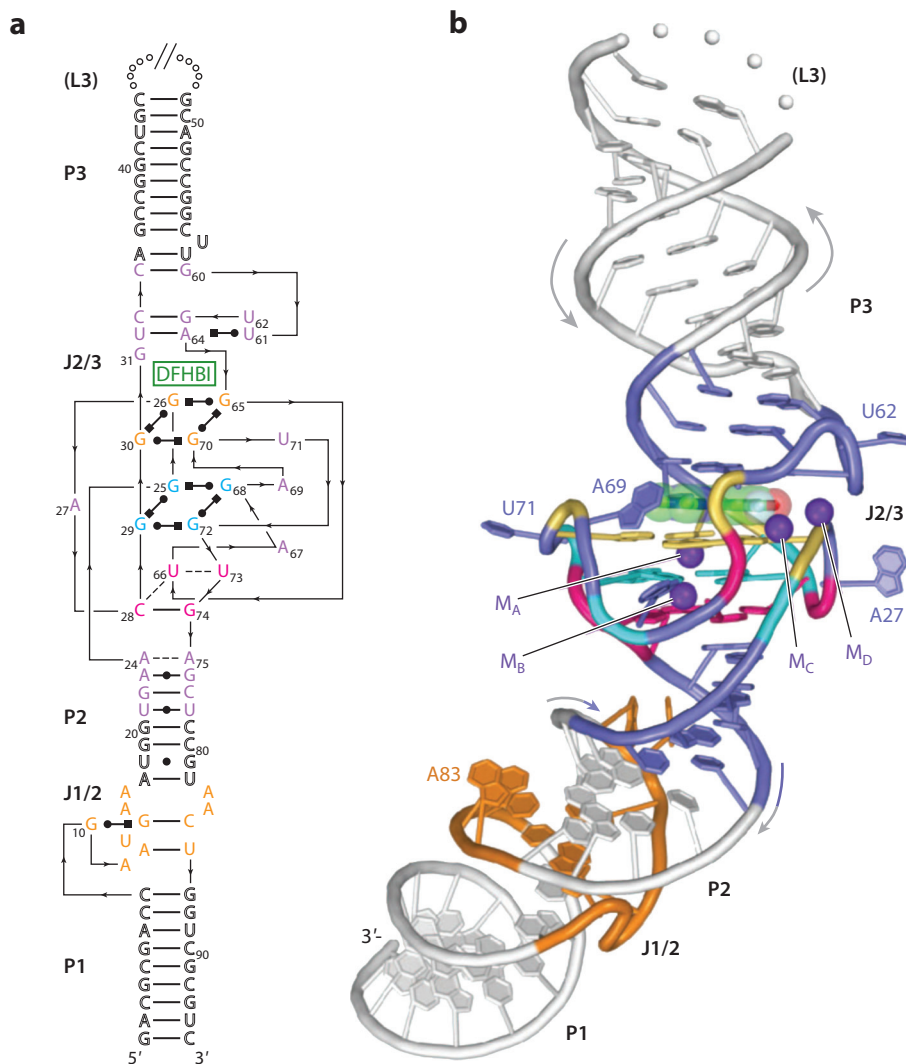


**Figure 4**

Structure of the Spinach–DFHBI complex. (a) Sequence and secondary structure of Spinach–DFHBI. The thin lines indicate chain connectivity; noncanonical base pairs are indicated with Leontis–Westhof symbols. Spinach folds into a single coaxial helical stack, which is ~110 Å long and contains three A-form duplexes (paired regions P1, P2, and P3). These duplexes are separated by two irregular junctions (J1/2 and J2/3). J2/3 forms the DFHBI binding domain, which contains a three-tetrad quadruplex comprising two G-quartets (*gold* and *cyan*) stacked above a mixed-sequence tetrad (*magenta*). The G-quartets are stabilized by two  $K^+$  ions ( $M_A$  and  $M_B$  in panel *b*). The DFHBI fluorophore is indicated in green. (b) Cartoon representation of the Spinach–DFHBI complex, color-coded as in panel *a*. The G-quartet that forms the base of the DFHBI binding pocket is indicated in gold. Purple spheres (labeled  $M_A$  through  $M_D$ ) represent  $K^+$  ions. Figure adapted with permission from Warner et al. (2014). *Nature Structural & Molecular Biology* 21:658–63, copyright 2014 by Macmillan Publishers, Ltd. Abbreviation: DFHBI, (Z)-4-(3,5-difluoro-4-hydroxybenzylidene)-1,2-dimethyl-1H-imidazol-5(4H)-one.

large enough to accommodate both DFHBI and other RNA moieties on the same plane, allowing additional coplanar interactions with the fluorophore (65).

### Possible Mechanisms of Improved DFHBI Quantum Yield after Spinach Binding

One important question in understanding the photophysics of the Spinach–DFHBI complex is as follows: How does Spinach bind to DFHBI and increase its quantum yield? At first glance, Spinach seems to enhance the behavior of DFHBI simply by binding to it and inhibiting isomerization around the methylene double bond. Indeed, the geometric restriction of DFHBI in a planar form between two planes composed of a G–quadruplex and a base triple can be an obvious explanation. It is also possible, however, that this simple packing constraint cannot account for the entire increase in quantum yield.

For example, the low quantum yield of DFHBI in the unbound state could result from relaxation from rotations around the bridging carbon bonds between two rings, but it could also result from nonradiative internal conversions from phenyl torsion or rotation around the imidazolinone bond or even excited-state intersystem crossing relaxation to the triplet state. In addition, when in the bound state, the charged RNA environment and hydrogen bonding interactions with the Spinach nucleic acids may alternately stabilize or destabilize the excited state of DFHBI and alternate the energy barrier during torsion or rotation around the bridging bond. Indeed, either a nearby negative charge around the electron acceptor or a nearby positive charge (e.g.,  $Mg^{2+}$ ) around the chromophore ring can decrease the electron transfer rate by destabilizing the charge transfer state, thus increasing the quantum yield. Excited-state decay measurements, including those generated by ultrafast fluorescence upconversion, polarization spectroscopy, and transient absorption spectroscopy, can be very useful for determining which mechanism dominates the suppression of nonradiative decay of the Spinach–DFHBI complex, as can calculations based on quantum chemical information, as evidenced in studies of GFP.

### Understanding the Photobleaching Properties of Spinach

The Spinach–DFHBI complex displays relatively fast fluorescence decay under continuous large-dose light irradiation (27, 64), which partially limits its application for imaging low-abundance RNA. In contrast to the irreversible photobleaching mechanism of GFP, however, the decreased fluorescence intensity of the Spinach–DFHBI complex seems more likely to stem from a reversible photoconversion to a less-fluorescent state. Two different groups (27, 64) have proposed that the photoinduced *cis*–*trans* isomerization of DFHBI may account for this behavior.

The first of these groups, Wang et al. (64), reported that under blue light irradiation, DFHBI undergoes *cis*–*trans* photoisomerization, and compared with the more fluorescent Spinach–*cis*-DFHBI complex, the Spinach–*trans*-DFHBI complex is threefold less stable and one-third dimmer. To improve the signal-to-background contrast during long-term imaging, an optical lock-in detection (OLID) scheme was proposed for imaging Spinach-based probes (64). Han et al. (27) further argued that the fast *cis*–*trans* photoisomerization induces fast unbinding of the DFHBI from Spinach, and a new ground-state DFHBI can again bind with Spinach to recover the fluorescence. This argument was supported by the strong dependence of the fluorescence recovery rate on the DFHBI concentration. As a result, a pulsed illumination scheme, instead of a regular continuous-wave illumination scheme, was proposed to help retain the high fluorescence signal of the Spinach–DFHBI complex, and the time between pulses was chosen to allow fresh DFHBI to bind and recover the fluorescence (27).

Even though these schemes improve the performance of Spinach-based probes during imaging, the use of new RNA–fluorophore complexes that have higher photostability will simplify imaging.

---

**Superresolution imaging:**

a microscopy method that images cellular structures at a higher resolution than that possible using traditional light microscopy methods

---

Increased photostability may be achieved by RNA aptamers that more efficiently suppress light-induced fluorophore dissociation or fluorophore isomerization. Photostability will be especially important for applications that require high-intensity irradiation, such as in single-molecule or superresolution imaging.

## USING SPINACH AND RELATED APTAMERS FOR IMAGING RNA IN LIVE CELLS

Spinach, Spinach2, and Broccoli can be used to tag RNAs for live-cell imaging in a manner analogous to the use of GFP-fusion proteins. In addition to expression in *E. coli* (46, 50, 54, 63), several RNAs have been expressed as fusion RNAs and imaged in mammalian cells, including 5S, a small ncRNA transcribed by RNA polymerase III that associates with the large ribosomal subunit (46); 7SK, an ncRNA that associates with transcription complexes; and CGG-repeat RNAs, which are linked to fragile X-associated tremor and ataxia syndrome (FXTAS) (57). In each case, fluorescence was not detectable in cells expressing a control RNA, whereas fluorescence was detected in cells expressing the imaging tag (57). In the case of 5S RNA, 5S–Spinach and 5S–Broccoli RNA fluorescence was detected throughout cells, with prominent fluorescence signals appearing as diffuse nuclear and cytosolic puncta (46). Fluorescence is particularly easy to detect after sucrose treatment, which leads to the formation of 5S RNA aggregates in the cytosol. These aggregates appear as distinctive puncta (46), and their distribution patterns are similar to those seen for endogenous 5S RNA in the same cell type (48). These data indicate that 5S–Spinach and 5S–Broccoli RNA fusions can be imaged in cells, including in the nucleus, and exhibit localizations consistent with endogenous RNA. Furthermore, the presence of the tag did not appear to affect the localization of the RNA for the RNAs tested (46, 57).

In contrast to eGFP, fluorescence is readily obtained after the Spinach RNA is synthesized, possibly ensuring that there are minimal temporal delays between RNA expression and RNA detection in living cells. Indeed, these tags can be used to image promoter activity using a FACS-based screen (19).

Several factors need to be considered when imaging RNA using Spinach in living cells. Imaging temperature could potentially influence fluorescence in living cells. Similarly, ion content in cells could affect imaging. Most RNAs are only able to achieve a folded structure at certain magnesium concentrations (10). Both Spinach and Spinach2 exhibit some magnesium dependence, and imaging is improved by adding exogenous magnesium to the culture media, which is expected to increase intracellular magnesium concentration. However, cells that exhibit low magnesium concentrations, or those that exhibit fluctuations in magnesium concentrations, could potentially influence the overall brightness or folding of Spinach. Broccoli exhibits reduced sensitivity to magnesium and is more thermostable than Spinach or Spinach 2, so this aptamer may be useful for overcoming the issues described above (19).

Another important consideration is aptamer folding. RNA aptamers are highly sensitive to adjacent sequences (39). Compared with Spinach, both Spinach2 and Broccoli show improved folding in diverse sequence contexts (19, 57). However, it is important to determine empirically whether the aptamer can fold properly when inserted into a target RNA. Therefore, an aptamer-tagged RNA should be synthesized *in vitro* before being expressed in living cells, and its molar fluorescence should be compared with that of a solution of the aptamer at the same concentration. These experiments should be performed in buffers that contain cytosolic ion concentrations. RNAs should only be expressed in living cells if the tagged RNA exhibits the expected fluorescence in solution. The development of so-called insulator sequences that provide a space between the target RNA and aptamers could also potentially reduce effects of the host RNA on aptamer folding.

Conceivably, aptamer insertion could also affect RNA stability; polyadenylation signals; or the function of microRNAs, which are typically located near the 3' end of the transcript (24). Thus, it may be important to compare the properties of the tagged RNA with those of the endogenous RNA to ensure the physiologic properties and functions of the host RNA are retained.

## **FUTURE DIRECTIONS**

### **Developing New Fluorescence Complexes Based On Non-HBI Fluorophores**

Studies have demonstrated that HBI-like fluorophores are powerful imaging tools when complexed with RNA aptamers such as Spinach or Broccoli. The issue of whether fluorophore structures other than those in the HBI family can undergo similar conditional fluorescence and be useful for imaging RNA in cells remains an open one. Dolgosheina et al. (17) recently reported the selection of an RNA aptamer, called RNA Mango, that binds thiazole orange derivatives with low-nanomolar binding affinity. After binding, the fluorescence signal increased by 1,100-fold (17). The thiazole orange dye is well known to exhibit high cellular background fluorescence due to nonspecific binding with cellular DNA and RNA, and it exhibits rapid photobleaching (53). However, the high binding affinity of RNA Mango can partially enhance the signal-to-noise ratio when imaging, as only small amount of dye is needed. Future studies can address whether Mango can be used as a tag for genetically encoding fluorescent RNA in living cells.

The most promising compounds for RNA-dependent activation are a group of fluorophores that have been named molecular rotors. When in the excited state, these compounds undergo a twisting motion that leads to extremely low-fluorescence quantum yields (25). Interestingly, the twisted-state relaxation rates (and thus the fluorescence intensities) of these molecules have been known to depend strongly on qualities of the local environment, such as viscosity or polarity (25). Structurally, these molecular rotors consist of an electron donor and an acceptor linked by  $\pi$  conjugation. Example molecules include triphenylmethane (e.g., malachite green); *p*-N,N-(dimethylamino)benzointrile (DMABN)-related structures (e.g., stilbenes); and [*p*-(dialkylamino)benzylidene]malononitrile (DBMN)-related structures (e.g., thioflavin T) (58). RNA aptamers could sterically inhibit the twisting motion or could tune the intramolecular charge transfer efficiency of the fluorophore between the twisted and local state. As a result, the excited twisted state would be unfavorable, leading to more radiative relaxation and thus enhanced quantum yield.

As mentioned above, unbound DFHBI displays very low cellular background fluorescence. However, low cellular background fluorescence is not seen with most other fluorophores, such as stilbene, triphenylmethane and cyanine dyes (23, 38). Indeed, even though aptamers that bind and activate the fluorescence of malachite green have been described (3), the high cellular background of this dye, as well as its ability to produce cytotoxic oxygen radicals, has limited the utility of these aptamers. The background fluorescence can be explained by partitioning into viscous membrane bilayers or nonspecific binding to cellular compounds. Background fluorescence due to nonspecific binding of thiazole orange to DNA was recently reduced by introducing a nitrile moiety that made the thiazole orange dye adopt a nonplanar configuration (53). Careful manipulation of fluorophore structures to minimize cellular interactions will be needed to ensure that new fluorophores used in RNA-fluorophore complexes have low background fluorescence.

### **Application of RNA-Fluorophore Complexes for Superresolution Imaging**

Imaging RNA at high resolution in living cells is critical for obtaining insight into the functions of different RNA-based structures. Many of these RNA structures, such as PML bodies, polycomb

bodies, Cajal bodies, and speckles, among others, are 1  $\mu\text{m}$  or smaller in size (56), however, making it difficult to accurately resolve their shape and size using regular imaging techniques.

Superresolution imaging techniques to circumvent the classical diffraction-limited resolution barrier in light microscopy have been recently developed. These techniques can provide information on, for example, the localization and structural information of GFP-labeled proteins at a resolution of 10 nm, compared with a resolution of  $\sim 400$  nm for epifluorescence microscopy (28). Fluorescent proteins have been applied in superresolution techniques such as stimulated emission depletion (STED) microscopy, and reversibly photoactivatable fluorescent proteins have been used to image protein structures with resolutions of less than 40 nm in photoactivated localization microscopy (PALM), stochastic optical reconstruction microscopy (STORM), and reversible saturable optically linear fluorescence transition (RESOLFT) microscopy (31, 33).

Superresolution imaging of RNA will require the RNA–fluorophore complexes to have several characteristics. Both high fluorescence brightness and high photostability during the on state are needed to generate enough photons to allow precise localization of single molecules. The reversible binding between RNAs and fluorophores can potentially provide the basis for the reversible transition between a fluorescent state and a dark state, thus breaking the diffraction barrier of imaging as used in STORM. RNAs bind and unbind fluorophores at specific  $k_{\text{on}}$  and  $k_{\text{off}}$  rates. The blinking rates of the photodeactivation ( $k_{\text{off}}$ ) and the photoactivation ( $k_{\text{on}}$ ) events should be balanced such that at a specific time, only a small portion of molecules are in the on state. In addition, the development of photoactivatable RNA–fluorophore complexes can be another important step in advancing RESOLFT-like superresolution RNA imaging. Considering the existence of several HBI fluorophore-based photoactivatable FPs, RNA–fluorophore complexes with similar photoactivation abilities can likely be developed. Indeed, as mentioned above, the observation of the fast, light-induced *cis*–*trans* isomerization of DFHBI indicates that the Spinach–DFHBI complex could potentially be evolved to be reversibly photoactivatable.

### SUMMARY POINTS

1. RNAs have highly complex and dynamic cellular localization patterns. RNA imaging in living cells is important for determining the function and regulation of both noncoding and coding RNAs.
2. Genetic encoding markedly simplifies RNA imaging. Although useful, current GFP–MS2 or split GFP–based RNA imaging methods have potential challenges that could limit their applications.
3. RNA imaging can be realized by tagging with an RNA aptamer sequence that activates the fluorescence of a fluorophore. These fluorophores should be bioorthogonal and exhibit fluorescence only when specifically bound to the aptamer.
4. RNA aptamers can bind and switch on the fluorescence of small-molecule derivatives of the GFP fluorophore, HBI. An RNA aptamer that activates the fluorescence of a fluorophore similar to the one in eGFP, DFHBI, was named Spinach.
5. Newer RNA–fluorophore complexes, such as Spinach2 and Broccoli, have been generated and have improved folding and cell compatibility. So-called plug-and-play fluorophores allow the spectral properties of Spinach2 and Broccoli to be adjusted on the basis of experimental needs.

6. The crystal structure of Spinach bound to DFHBI reveals that fluorescence is achieved by forcing DFHBI planarity via sandwiching it between a G-quadruplex and a planar U-A-U base triple.
7. Spinach, Spinach2, and Broccoli can be used to tag RNAs for live-cell imaging. Several RNAs including 5S, 7SK, and CGG-repeat RNAs have been expressed and imaged in mammalian cells.

## FUTURE ISSUES

1. Why does the Spinach-based complex display fast fluorescence decay under high-intensity light irradiation? How can its photostability be improved? How can new photostable RNA–fluorophore complexes be evolved?
2. Can new RNA–fluorophore complexes be generated to exhibit highly efficient red fluorescence, similar to what is seen with red fluorescent proteins?
3. How can the cellular behavior of RNA–fluorophore complexes be further improved to achieve high expression levels, efficient folding, and high stability?
4. Can the brightness and cellular performance of these aptamer tags be improved to image single RNA molecules in vivo?
5. Can fluorophores that are not based on HBI be developed, and what properties can these fluorophores confer to improve RNA imaging?
6. Can RNA–fluorophore complexes be developed that achieve the special requirements needed for superresolution imaging?

## DISCLOSURE STATEMENT

Samie R. Jaffrey is a cofounder of Lucerna Technologies and is an author of patent applications related to Spinach and related aptamers. M.Y. is not aware of any affiliations, memberships, funding, or financial holdings that might be perceived as affecting the objectivity of this review.

## ACKNOWLEDGMENTS

We thank members of the Jaffrey lab for helpful comments and suggestions. This work was supported by National Institutes of Health grants to S.R.J. (R01 NS064516 and R01 EB010249).

## LITERATURE CITED

1. Anderson P, Kedersha N. 2002. Visibly stressed: the role of eIF2, TIA-1, and stress granules in protein translation. *Cell Stress Chaperones* 7:213–21
2. Aravin A, Gaidatzis D, Pfeffer S, Lagos-Quintana M, Landgraf P, et al. 2006. A novel class of small RNAs bind to MILI protein in mouse testes. *Nature* 442:203–7
3. Babendure JR, Adams SR, Tsien RY. 2003. Aptamers switch on fluorescence of triphenylmethane dyes. *J. Am. Chem. Soc.* 125:14716–17
4. Baffour-Awuah NA, Zimmer M. 2004. Hula-twisting in green fluorescent protein. *Chem. Phys.* 303:7–11

5. Bagni C, Greenough WT. 2005. From mRNP trafficking to spine dysmorphogenesis: the roots of fragile X syndrome. *Nat. Rev. Neurosci.* 6:376–87
6. Batista PJ, Chang HY. 2013. Long noncoding RNAs: cellular address codes in development and disease. *Cell* 152:1298–307
7. Beermann AE, Jay DG. 1994. Chromophore-assisted laser inactivation of cellular proteins. *Methods Cell Biol.* 44:715–32
8. Bertrand E, Chartrand P, Schaefer M, Shenoy SM, Singer RH, Long RM. 1998. Localization of ASH1 mRNA particles in living yeast. *Mol. Cell* 2:437–45
9. Bokman SH, Ward WW. 1981. Renaturation of *Aequorea* green-fluorescent protein. *Biochem. Biophys. Res. Commun.* 101:1372–80
10. Brion P, Westhof E. 1997. Hierarchy and dynamics of RNA folding. *Annu. Rev. Biophys. Biomol. Struct.* 26:113–37
11. Carlile TM, Rojas-Duran MF, Zinshteyn B, Shin H, Bartoli KM, Gilbert WV. 2014. Pseudouridine profiling reveals regulated mRNA pseudouridylation in yeast and human cells. *Nature* 515:143–46
12. Chudakov DM, Matz MV, Lukyanov S, Lukyanov KA. 2010. Fluorescent proteins and their applications in imaging living cells and tissues. *Physiol. Rev.* 90:1103–63
13. Clore GM, Gronenborn AM. 1985. Probing the three-dimensional structures of DNA and RNA oligonucleotides in solution by nuclear Overhauser enhancement measurements. *FEBS Lett.* 179:187–98
14. Cody CW, Prasher DC, Westler WM, Prendergast FG, Ward WW. 1993. Chemical structure of the hexapeptide chromophore of the *Aequorea* green-fluorescent protein. *Biochemistry* 32:1212–18
15. De S, Girigoswami A, Mandal S. 2002. Enhanced fluorescence of triphenylmethane dyes in aqueous surfactant solutions at supramicellar concentrations—effect of added electrolyte. *Spectrochim. Acta A* 58:2547–55
16. Derrien T, Johnson R, Bussotti G, Tanzer A, Djebali S, et al. 2012. The GENCODE v7 catalog of human long noncoding RNAs: analysis of their gene structure, evolution, and expression. *Genome Res.* 22:1775–89
17. Dolgosheina EV, Jeng SCY, Panchapakesan SSS, Cojocaru R, Chen PSK, et al. 2014. RNA Mango aptamer-fluorophore: a bright, high-affinity complex for RNA labeling and tracking. *ACS Chem. Biol.* 9:2412–20
18. Famulok M, Mayer G, Blind M. 2000. Nucleic acid aptamers—from selection in vitro to applications in vivo. *Acc. Chem. Res.* 33:591–99
19. **Filonov GS, Moon JD, Svensen N, Jaffrey SR. 2014. Broccoli: rapid selection of an RNA mimic of green fluorescent protein by fluorescence-based selection and directed evolution. *J. Am. Chem. Soc.* 136:16299–308**
20. Gold L, Polisky B, Uhlenbeck O, Yarus M. 1995. Diversity of oligonucleotide functions. *Annu. Rev. Biochem.* 64:763–97
21. Grate D, Wilson C. 1999. Laser-mediated, site-specific inactivation of RNA transcripts. *PNAS* 96:6131–36
22. Green R, Ellington AD, Szostak JW. 1990. In vitro genetic analysis of the *Tetrahymena* self-splicing intron. *Nature* 347:406–8
23. Guidry G. 1999. A method for counterstaining tissues in conjunction with the glyoxylic acid condensation reaction for detection of biogenic amines. *J. Histochem. Cytochem.* 47:261–64
24. Hafner M, Landthaler M, Burger L, Khorshid M, Hausser J, et al. 2010. Transcriptome-wide identification of RNA-binding protein and microRNA target sites by PAR-CLIP. *Cell* 141:129–41
25. Haidekker MA, Theodorakis EA. 2010. Environment-sensitive behavior of fluorescent molecular rotors. *J. Biol. Eng.* 4:11
26. Han J, Kim D, Morris KV. 2007. Promoter-associated RNA is required for RNA-directed transcriptional gene silencing in human cells. *PNAS* 104:12422–27
27. **Han KY, Leslie BJ, Fei J, Zhang J, Ha T. 2013. Understanding the photophysics of the Spinach-DFHBI RNA aptamer-fluorogen complex to improve live-cell RNA imaging. *J. Am. Chem. Soc.* 135:19033–38**
28. Hell SW. 2009. Microscopy and its focal switch. *Nat. Methods* 6:24–32
29. Hesselberth JR, Miller D, Robertus J, Ellington AD. 2000. In vitro selection of RNA molecules that inhibit the activity of ricin A-chain. *J. Biol. Chem.* 275:4937–42

---

19. Describes directed evolution of RNA-fluorophore complexes and the generation of Broccoli.

---



---

27. Describes a photophysical study of the photobleaching and photoconversion of the Spinach-DFHBI complex.

---

30. Hocine S, Raymond P, Zenklusen D, Chao JA, Singer RH. 2013. Single-molecule analysis of gene expression using two-color RNA labeling in live yeast. *Nat. Methods* 10:119–21
31. Hofmann M, Eggeling C, Jakobs S, Hell SW. 2005. Breaking the diffraction barrier in fluorescence microscopy at low light intensities by using reversibly photoswitchable proteins. *PNAS* 102:17565–69
32. Holeman LA, Robinson SL, Szostak JW, Wilson C. 1998. Isolation and characterization of fluorophore-binding RNA aptamers. *Fold. Des.* 3:423–31
33. Huang B, Bates M, Zhuang X. 2009. Super-resolution fluorescence microscopy. *Annu. Rev. Biochem.* 78:993–1016
34. **Huang H, Suslov NB, Li NS, Shelke SA, Evans ME, et al. 2014. A G-quadruplex-containing RNA activates fluorescence in a GFP-like fluorophore. *Nat. Chem. Biol.* 10:686–91**
35. Kiebler MA, Bassell GJ. 2006. Neuronal RNA granules: movers and makers. *Neuron* 51:685–90
36. Kojima S, Ohkawa H, Hirano T, Maki S, Niwa H, et al. 1998. Fluorescent properties of model chromophores of tyrosine-66 substituted mutants of *Aequorea* green fluorescent protein (GFP). *Tetrahedron Lett.* 39:5239–42
37. Kummer AD, Kompa C, Lossau H, Pollinger-Dammer F, Michel-Beyerle ME, et al. 1998. Dramatic reduction in fluorescence quantum yield in mutants of Green Fluorescent Protein due to fast internal conversion. *Chem. Phys.* 237:183–93
38. Likhtshtein GI, Bishara R, Papper V, Uzan B, Fishov I, et al. 1996. Novel fluorescence-photochrome labeling method in the study of biomembrane dynamics. *J. Biochem. Biophys. Methods* 33:117–33
39. Martell RE, Nevins JR, Sullenger BA. 2002. Optimizing aptamer activity for gene therapy applications using expression cassette SELEX. *Mol. Ther.* 6:30–34
40. Meech SR. 2009. Excited state reactions in fluorescent proteins. *Chem. Soc. Rev.* 38:2922–34
41. Merzlyak EM, Goedhart J, Shcherbo D, Bulina ME, Shcheglov AS, et al. 2007. Bright monomeric red fluorescent protein with an extended fluorescence lifetime. *Nat. Methods* 4:555–57
42. Meyer KD, Saletore Y, Zumbo P, Elemento O, Mason CE, Jaffrey SR. 2012. Comprehensive analysis of mRNA methylation reveals enrichment in 3' UTRs and near stop codons. *Cell* 149:1635–46
43. Mhlanga MM, Tyagi S. 2006. Using tRNA-linked molecular beacons to image cytoplasmic mRNAs in live cells. *Nat. Protoc.* 1:1392–98
44. Niwa H, Inouye S, Hirano T, Matsuno T, Kojima S, et al. 1996. Chemical nature of the light emitter of the *Aequorea* green fluorescent protein. *PNAS* 93:13617–22
45. Ormö M, Cubitt AB, Kallio K, Gross LA, Tsien RY, Remington SJ. 1996. Crystal structure of the *Aequorea victoria* green fluorescent protein. *Science* 273:1392–95
46. **Paige JS, Wu KY, Jaffrey SR. 2011. RNA mimics of green fluorescent protein. *Science* 333:642–46**
47. Parker R, Song H. 2004. The enzymes and control of eukaryotic mRNA turnover. *Nat. Struct. Mol. Biol.* 11:121–27
48. Paul CP, Good PD, Li SXL, Kleihauer A, Rossi JJ, Engelke DR. 2003. Localized expression of small RNA inhibitors in human cells. *Mol. Ther.* 7:237–47
49. Ponchon L, Dardel F. 2007. Recombinant RNA technology: the tRNA scaffold. *Nat. Methods* 4:571–76
50. Pothoulakis G, Ceroni F, Reeve B, Ellis T. 2013. The Spinach RNA aptamer as a characterization tool for synthetic biology. *ACS Synth. Biol.* 3:182–87
51. Remington SJ. 2011. Green fluorescent protein: a perspective. *Protein Sci.* 20:1509–19
52. Sando S, Narita A, Hayami M, Aoyama Y. 2008. Transcription monitoring using fused RNA with a dye-binding light-up aptamer as a tag: a blue fluorescent RNA. *Chem. Commun.* 33:3858–60
53. Shank NI, Pham HH, Waggoner AS, Armitage BA. 2013. Twisted cyanines: a non-planar fluorogenic dye with superior photostability and its use in a protein-based fluoromodule. *J. Am. Chem. Soc.* 135:242–51
54. Shu D, Khisamutdinov EF, Zhang L, Guo P. 2014. Programmable folding of fusion RNA in vivo and in vitro driven by pRNA 3WJ motif of phi29 DNA packaging motor. *Nucleic Acids Res.* 42:e10
55. Song W, Strack RL, Svendsen N, Jaffrey SR. 2014. Plug-and-play fluorophores extend the spectral properties of Spinach. *J. Am. Chem. Soc.* 136:1198–201
56. Spector DL, Lamond AI. 2011. Nuclear speckles. *Cold Spring Harb. Perspect. Biol.* 3:a000646
- 
34. Describes the crystal structure of the Spinach–DFHBI complex and provides insights into the mechanism of fluorescence activation (see also Reference 65).
- 
46. Describes the initial generation of Spinach for RNA imaging.
-

---

57. Describes the generation of Spinach2, a Spinach variant with improved folding and imaging properties.

---

57. Strack RL, Disney MD, Jaffrey SR. 2013. A superfolding Spinach2 reveals the dynamic nature of trinucleotide repeat RNA. *Nat. Methods* 10:1219–24
58. Stsiapura VI, Maskevich AA, Kuzmitsky VA, Uversky VN, Kuznetsova IM, Turoverov KK. 2008. Thioflavin T as a molecular rotor: fluorescent properties of thioflavin T in solvents with different viscosity. *J. Phys. Chem. B* 112:15893–902
59. Tsien RY. 1998. The green fluorescent protein. *Annu. Rev. Biochem.* 67:509–44
60. Tyagi S. 2009. Imaging intracellular RNA distribution and dynamics in living cells. *Nat. Methods* 6:331–38
61. Tyagi S, Alsmadi O. 2004. Imaging native  $\beta$ -actin mRNA in motile fibroblasts. *Biophys. J.* 87:4153–62
62. Valencia-Burton M, McCullough RM, Cantor CR, Broude NE. 2007. RNA visualization in live bacterial cells using fluorescent protein complementation. *Nat. Methods* 4:421–27
63. van Nies P, Nourian Z, Kok M, van Wijk R, Moeskops J, et al. 2013. Unbiased tracking of the progression of mRNA and protein synthesis in bulk and in liposome-confined reactions. *ChemBioChem* 14:1963–66
64. Wang P, Querard J, Maurin S, Nath SS, Le Saux T, et al. 2013. Photochemical properties of Spinach and its use in selective imaging. *Chem. Sci.* 4:2865–73
65. Warner KD, Chen MC, Song W, Strack RL, Thorn A, et al. 2014. Structural basis for activity of highly efficient RNA mimics of green fluorescent protein. *Nat. Struct. Mol. Biol.* 21:658–63
66. Yang F, Moss LG, Phillips GN Jr. 1996. The molecular structure of green fluorescent protein. *Nat. Biotechnol.* 14:1246–51
67. Zhang X, Potty AS, Jackson GW, Stepanov V, Tang A, et al. 2009. Engineered 5S ribosomal RNAs displaying aptamers recognizing vascular endothelial growth factor and malachite green. *J. Mol. Recognit.* 22:154–61